Image Cover Sheet

CLASSIFICATION	SYSTEM NUMBER
UNCLASSIFIED	512641

TITLE

Particle Distributions and Index of Refraction Estimation for Canadian Waters

System Number:

Patron Number:

Requester:

Notes:

DSIS Use only:

Deliver to:

PROCEEDINGS OF SPIE REPRINT

SPIE—The International Society for Optical Engineering

Reprinted from

Airborne and In-Water Underwater Imaging

21–22 July 1999
Denver, Colorado

SPIE
P
PROCEEDINGS SERIES

Volume 3761

Particle distributions and index of refraction estimation for Canadian waters

J.L. Forand and G.R. Fournier

Defence Research Establishment Valcartier
2459 Pie-XI North, Val-Belair, Quebec, G3J 1X5, Canada

ABSTRACT

Extensive measurements were carried out of the optical properties of seawater off the East and West Coasts of Canada using a full-spectrum near-forward angle nephelometer (NEARSCAT). Using a new phase function adapted specifically to scattering from water borne particles, we analyze the data from coastal waters in the Straits of Juan de Fuca and in the Gulf of St-Lawrence. We show explicitly how the spectral properties can be combined with the angular properties to more reliably extract the Junge exponent of the particle size distribution and the mean index of refraction of the particles. We obtain a simple analytic expression for the normalized cumulative phase function that can be used to compute the backscatter ratio, and its explicit wavelength dependence. Accurate estimation of this wavelength dependence is required for accurate hyper-spectral image prediction.

Keywords: propagation, scattering, underwater, phase function, coastal

1. INTRODUCTION

Some time ago we derived a phase function approximation for oceanic waters[1] that correctly modeled the near forward angle behavior of measured phase functions. A significant drawback of this function was that it could not be easily normalized. A simple modification has allowed us to remove this drawback and produce analytic forms both for the normalized phase function and for its cumulative integral. In this new form the function can be used to extract reliable information about the exponent of the power law of the particle size distribution and the mean index of refraction of the scattering particles. We will show that a power law for the particle size distribution implies a corresponding power law for the wavelength dependence of the scattering and gives rise to a related angular power law in the small angle limit of the phase function. We will then use these relationships and the derived expressions for the cumulative integral of the phase functions to reanalyze the measurements that we carried out on the coasts of Canada with a full-spectrum near-forward angle nephelometer (NEARSCAT) [2,3].

2. DERIVATION OF AN OCEANIC PHASE FUNCTION

To obtain the phase function of an ensemble of spherical particles one must perform the following integral.

$$\beta(\vartheta) = \int_0^\infty \pi r^2 \, Q(x) P(\theta, x) F(r) dr \tag{1}$$

In equation 1, r is the particle radius and $x = 2\pi r / \lambda$ the particle size parameter, λ is the wavelength of the illuminating source in the medium surrounding the particles. $Q(x)$ is the scattering efficiency which is defined as the ratio of the particle scattering cross-section to the geometric cross-section. $P(\vartheta, x)$ is the single particle scattering function normalized to unity when integrated over 4π steradians and $F(r)$ is the particle size distribution function. It has been noted that to a first approximation the measured particle size distributions in the ocean follow an inverse power law (Junge distribution).

$$F(r) = \frac{C}{r^\mu}$$

Part of the SPIE Conference on Airborne and In-Water Underwater Imaging
Denver, Colorado • July 1999
SPIE Vol. 3761 • 0277-786X/99/$10.00

Assuming a distribution of this type it is instructive to write equation 1 in terms of the particle size parameter x.

$$\beta(\vartheta) = C(2\pi/\lambda)^{\mu-3}\pi\int_0^\infty Q(x)P(\theta,x)x^{2-\mu}dx \tag{2}$$

Note the very important fact that equation 2 predicts an inverse power relationship as a function of wavelength for the total scattering coefficient. This relationship is purely a property of the particle size distribution function, independent of the particle shape. The only requirement is that the index also be independent of wavelength over the range of interest. The wavelength dependence of the scattering coefficient is therefore dictated by the particle size distribution in this case. This allows us to wavelength interpolate and extrapolate scattering coefficients on a very firm basis.

From a further analysis of equation 2 we can show that for small finite angles the scattering coefficient behaves as an inverse power of θ. Chen[4] has recently shown that, to a good approximation, for large particles with modest indices of refraction

$$P(\theta,x) = N(x)p(2x\sin(\theta/2)) \tag{3}$$

$N(x)$ is the normalization factor obtained when one integrates the scattering function over the sphere and $p(\theta,x)$ is the un-normalized scattering function. If we now define two new variables $u = 2\sin(\vartheta/2)$ and $z = xu$ then substitute them in equation 2, we obtain:

$$\beta(\theta) = C(2\pi/\lambda)^{\mu-3}\pi u^{\mu-3}\int_0^\infty Q(z/u)\,N(z/u)\,p(z)\,z^{2-\mu}dz \tag{4}$$

The angular dependence of the kernel of equation 4 is now completely contained in the normalization factor $N(z,u)$ and in the scattering efficiency term $Q(z,u)$. In the case of large particles, which dominate the scattering in the near forward direction, Babinet's principle states that

$$Q = 2$$

We also find that

$$N(z/u) \propto z^2/u^2 = x^2$$

This last relationship occurs because the width of the forward diffraction peak of a finite object narrows as the inverse of the square of the characteristic size parameter x and therefore the normalized amplitude must increase as the square of x. This scaling law is purely due to the wave nature of light and will apply even in the case of irregularly shaped particles with the proviso that the size parameter be replaced by some effective size parameter such as that of the volume equivalent sphere. Substituting these general asymptotic relationships into equation 4 we obtain:

$$\beta(\theta) \propto (2\pi/\lambda)^{\mu-3}\pi[2\sin(\theta/2)]^{\mu-5} = (2\pi/\lambda)^{\gamma}\pi[2\sin(\theta/2)]^{\eta} \tag{5}$$

Equation 5 shows that, given an inverse power law particle size distribution, the small angle forward scattering will also vary as an inverse power law in θ. Equation 5 also shows clearly the extremely close relationship that exists between the exponent of the spectral dependence and the exponent of the angular dependence of the scattering coefficient. Both exponents can be related to one another as follows:

$$\gamma = \eta + 2 \tag{6}$$

Equation 6 shows clearly the remarkable fact that by measuring the logarithmic slope of the scattering coefficient near zero degrees η at one wavelength, we can compute the full spectral dependence of the scattering coefficient and the value of the exponent of its power law γ. Equation 6 is all the more remarkable because it was derived from general scattering principles without explicit reference to any specific shape properties of the particles. It is a direct consequence of the assumption that an inverse power law is an adequate model for oceanic size distribution functions. As we shall see later it is particularly useful in the analysis of our nephelometric data, as the near forward angle is precisely the zone that NEARSCAT measures.

As a matter of completeness it should be noted that the convolution of the instrumental angular response function with equation 5 avoids the occurrence of singularities at precisely the forward angle. Because of this convolution, even a perfect nephelometer operated very near the forward direction will measure the angular diffraction limit of its aperture as the point where a roll over from the inverse power law occurs.

Using some simple approximations for the extinction efficiency and for the single particle phase function, we have previously[1] shown how to integrate equation 4 to obtain an analytic formula for oceanic scattering. We will only repeat here the key parts of the derivation along with corrections to a few misprints that had slipped by in our previous work. We fist assume that

$$Q(x) \approx \frac{\rho^2/2}{1+\rho^2/4} \quad , \quad \rho = 2(n-1)x \tag{7}$$

$$P(\theta,x) \approx \frac{1}{4\pi}\frac{(1+4x^2/3)}{(1+u^2x^2/3)^2} \quad , \quad u = 2\sin(\theta/2) \tag{8}$$

Using equations 7, 8 and 2, we first compute the total scattering coefficient. According to our previous discussion it will be a function of the wavelength, the Junge exponent of the particle size distribution and the index of refraction n.

$$b(\lambda,\mu,n) = C(2\pi/\lambda)^{\mu-3}\pi\int_0^\infty Q(x)\,x^{2-\mu}dx \tag{9}$$

$$b(\lambda,\mu,n) = C\frac{\pi}{\cos(\pi\mu/2)}\left(\frac{2\pi(n-1)}{\lambda}\right)^{\mu-3} \tag{10}$$

If we now define the normalized phase function as

$$b(\theta) = \frac{\beta(\theta)}{b(\lambda,\mu,n)}$$

then

$$b(\theta) = \frac{1}{4\pi}\frac{1}{(1-\delta)^2\delta^\nu}\left(\left[\nu(1-\delta)-(1-\delta^\nu)\right]+\frac{4}{u^2}\left[\delta(1-\delta^\nu)-\nu(1-\delta)\right]\right) \tag{11}$$

where

$$\nu = \frac{3-\mu}{2} \quad , \quad \delta = \frac{u^2}{3(n-1)^2} \quad , \quad u = 2\sin(\theta/2)$$

Equation 11 is different from our previous work in that we have not explicitly used the polarization dependence. We have found that it prevents one from obtaining a simple analytic expression for the normalization integrals. The effect of this term is only noticeable at large angles where the contribution from small particles dominates the phase function. As we shall see, the polarization dependence can be introduced as a correction term at a later stage. We now define the normalized cumulative probability distribution of scattering as:

$$w(\theta) = 2\pi\int_0^\theta b(\theta')\sin(\theta')\,d\theta' \tag{12}$$

Upon substitution of equation 11 in equation 12 we obtain:

$$w(\theta) = \frac{1}{(1-\delta)\delta^\nu}\left[(1-\delta^{\nu+1})-\frac{u^2}{4}(1-\delta^\nu)\right] \tag{13}$$

As was mentioned previously one further step is required to reintroduce the polarization effects at the large angles. In order to achieve this without destroying the simple normalization properties of our functions we will first subtract from equation 11 a constant equal to $b(\pi)$ and then add back a polarization term with the same angle integrated value of $4\pi\,b(\pi)$. Doing this, we obtain the following final formulae:

$$b_f(\theta) = b(\theta) + b(\pi)\frac{[3\cos^2(\theta) - 1]}{4} \quad (14)$$

$$w_f(\theta) = w(\theta) + w(\pi)\frac{\pi\cos(\theta)\sin^2(\theta)}{2} \quad (15)$$

Equations 14 and 15 along with the normalization equation 10 are the final formulae used in the analysis of our data.

3. EXPERIMENTAL VERIFICATION OF THE PHASE FUNCTION

There are very few complete marine phase function data sets that combine measurements at both large and small angles. The data of Petzold[5] stands out in this respect. It is probably the most complete data set in terms of angular coverage but unfortunately for our purposes the data was measured at only one wavelength. The only data set that adequately covers both angular and wavelength range is that of Whitlock[6] for turbid estuary waters. Using a moored buoy, the phase functions were measured simultaneously at 50 nm intervals from 450 nm to 800 nm. This set covers a sufficiently wide angular and wavelength range to be an excellent test of the concepts outlined in the previous section. We first performed a fit to each phase function using a standard non-linear simplex algorithm[7-8] that minimized the relative least squares error. The formula used in this fit was:

$$B(\theta) = Ab_f(\theta) \quad (16)$$

where the parameters to fit are the total scattering amplitude A, the index of refraction and the power of the particle size distribution μ. The result of this fit at a wavelength of 800 nm is shown in figure 1. The relative RMS error is less than 8% showing the close match of our functional form to the phase functions at each wavelength.

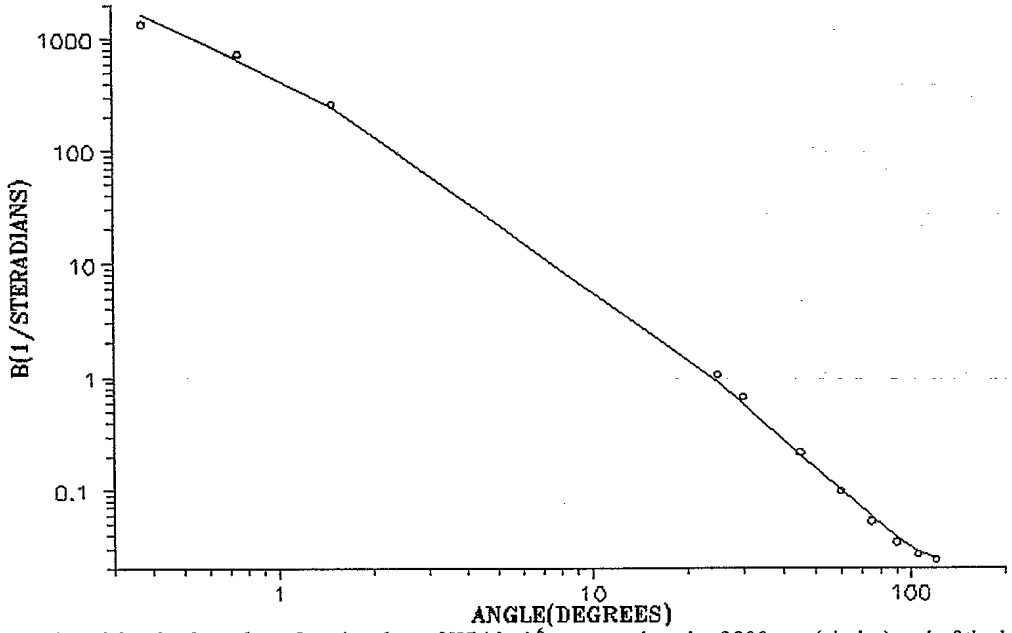

Figure 1. Plot of the absolute phase function data of Whitlock[6] at a wavelength of 800 nm (circles) and of the best fit using our phase function formula (solid line, $\mu = 3.77, n = 1.09$).

We also performed a fit to the entire set of phase functions using the wavelength dependence given in equation (5). The following equation was used for this second fit:

$$B(\theta) = A_t\left(\frac{\lambda_r}{\lambda}\right)^{\mu-3} b_f(\theta) \quad (17)$$

where λ_r is an arbitrary reference wavelength which we chose to be 550 nm and A_t is the total amplitude. The results of this overall fit are compared with the parameters obtained from the single wavelength fits in figure 2. The solid line is the result of the overall fit and for comparison the dotted line is the least squares fit of an arbitrary power law as a function of wavelength. The close agreement between these two clearly shows that our overall formula is also the best fit to the total scattering cross-section as a function of wavelength and completely validates formula 17.

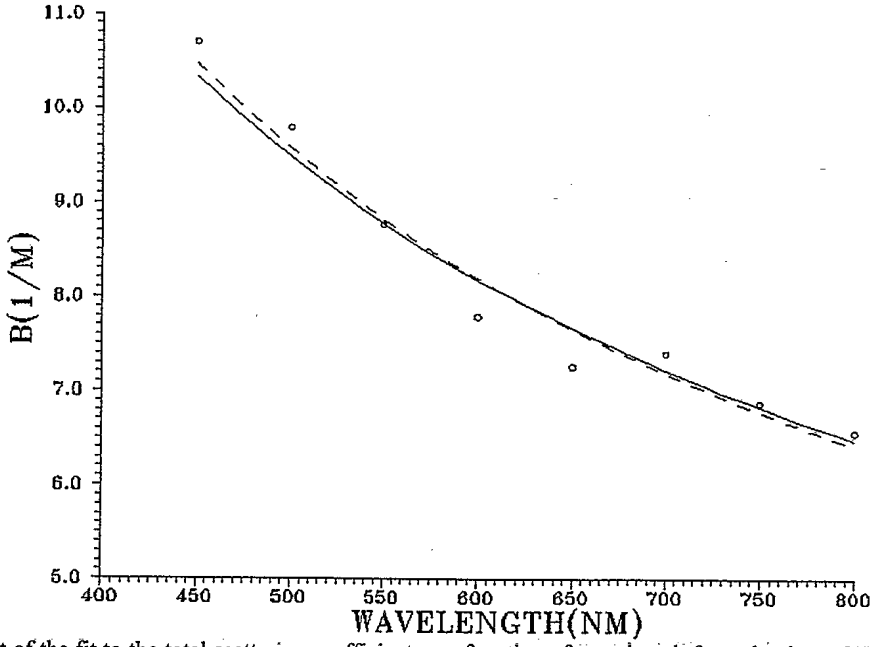

Figure 2. Plot of the fit to the total scattering coefficient as a function of wavelength from the data of Whitlock[6]. The circles represent the results of independent fits of the phase function at each wavelength. The solid line is the result of the simultaneous fit of all wavelengths using formula 17 ($\mu = 3.79, n = 1.08$). The dashed line is the result of a power law least squares fit to the data represented by the circles.

As was mentioned previously, there are very few data sets that incorporate both near forward angle and large angle data points. The combination of both is required to obtain reliable values of μ and index of refraction. Therefore we carefully analyzed the full data sets of Petzold[5] and Whitlock[6]. We first corrected the data to take out the scattering due to pure seawater using the formula derived by Morel[9]. After this correction and eliminating a single result that was an obvious outlier, a remarkable regularity was found. The index of refraction of the scattering particles was centered at a mean value of 1.09 with a very tight standard deviation of 0.01. The mean value of μ was 3.649 with a standard deviation of 0.123.

4. NEAR FORWARD ANGLE NEPHELOMETER

Several years ago we built NEARSCAT, a multispectral near-forward-angle nephelometer[2,3]. It was designed to perform essentially simultaneous measurements at many wavelengths. Measurements at all scattering angles would have required an instrument whose mechanical motion would have been too slow to insure a continuous scan of multiple wavelengths. However, because well over one third to one half of the integrated scatter in seawater occurs in the first 30 mrad, it is possible, by judicious extrapolation using a sound theoretical phase function, to accurately estimate the total scatter. NEARSCAT uses four angular channels: a central channel, extending from 0 to 4.7 mrad, to measure both the transmitted and scattered signal, and three concentric annular rings to measure the scattered signal out to an angle of 26 mrad. The data from these four channels is used to calculate the extinction coefficient and to estimate the scattering coefficient using a fit to a two parameter phase function. The absorption coefficient is then given by the difference between the extinction and scattering coefficients. For practical reasons, the instrument's path length was limited to 50 cm. With the instrument, attenuation lengths up to 50 m can be reliably measured. In that case, to obtain a relative accuracy of 10%, the transmissometer must be able to make measurements one part in a thousand or better. NEARSCAT has demonstrated a reliability of one part in two thousand.

NEARSCAT is a computer-controlled probe that consists of three main sections (Fig. 3). The emitter section contains a computer-controlled monochromator that produces a tightly collimated beam of light. The water sampling section is constructed to allow free flow of water while baffling the beam zone from external light sources. The receiver section has four optical channels that are used to monitor both the directly transmitted light and the light scattered into three different solid-angle bands. For the sake of clarity only two of the three scattering channels are shown in figure 3. In addition, the probe has sensors for determining its depth and the temperature of the water. An onboard microprocessor controls every aspect of its operation.

White light from one of two operator-selectable quartz-halogen lamps is collimated by a 20-cm focal length surface-coated mirror and directed onto a 1200 lines per millimeter replica grating blazed at 500 nm. The grating, mounted on a ballistic galvanometer, can be set to any wavelength between 400 and 700 nm in less than 20 ms with reproducibility better than 1 nm. The light dispersed by the grating is refocused onto a 2-mm diameter iris situated at the focal plane of the 20-cm focal length exit mirror. Neglecting the width of the lamp filament's image, the monochromator behaves, to first order, as a spectral filter with a resolution of 10 nm. Changing the diameter of the iris changes the spectral resolution. A 600 Hz synchronized chopping wheel (chopper) is positioned immediately after the output iris of the monochromator. This frequency was chosen because it gives the best signal-to-noise ratio for the photodiode and transimpedance amplifier combination used for the detectors. Positioned after the chopper, an un-coated quartz beam splitter sends a small percentage of the light to a lens, which loosely focuses it onto a photodiode. This reference signal is used to monitor the instantaneous light intensity for later normalisation. The remainder of the light is re-collimated, such that the half-angle divergence of the output beam in water is 2.15 mr before passing through a quartz window and entering the water sampling section. Light baffles are spaced 5 cm apart and positioned to isolate the section from all external light sources while not impeding the free flow of water through the section. The production of flow eddies is reduced by flush-mounting the quartz windows. Baffling is required to prevent light from external sources from entering into the optical system and causing the detectors to saturate.

After traversing the water sampling section, the beam enters the receiver section. Here, the beam is divided into four parts by a set of three 50 % cube beam splitters and focused onto four different iris diaphragms. The circular iris for the direct transmission channel has a diameter of 5 mm. The irises for the scattering channels are ring apertures. An f/1 aspheric lens is positioned behind each iris to image the entrance plane of the primary focusing lens onto the photodiodes. As the irises are at the focal plane of the primary lens, a linear relationship exists between the radius of the iris aperture and the angle of the light after it has traversed the water sampling section. As a result, each diode receives light that has been scattered or transmitted into a well-defined range of solid angles. The signal from the diode is amplified, filtered, rectified, and integrated before being converted to a digital signal.

The onboard microprocessor is used as the controlling interface between a shipboard computer and the NEARSCAT probe. A two-way communication link and software package allows the user to send instructions to the probe, to monitor the probe's status, to view all the raw data in real time, to save the data to disk, and to review the data at a later time in both text and graphic formats.

The amount of light collected by each of the probe's detectors can be calculated using the single scattering paraxial approximation. However, as the transmissometer is not optically perfect, a parasitic scattering term needs to be added. The contribution from the quartz windows to this parasitic signal in the scattering channels was determined to be negligible by measuring their signals with and without the windows in place. As a result, the normalised signals can be expressed by:

$$r_0 S_0 = r_0 S^0 e^{-(a+s)l}\left[1 + sl\ w_f(\theta_0)\right] \tag{18}$$

$$r_n S_n = r_0 S^0 e^{-(a+s)l} sl\left[w_f(\theta_{iu}) - w_f(\theta_{il})\right] + r_n S^n e^{-(a+s)l} \tag{19}$$

where the second term in equation 19 is the parasitic contribution. The angles θ_{il} and θ_{iu} are the inner and outer angles for the ith iris and θ_0 is the outer angle for the central iris. The normalised signals, S^n (n=0,1,2,3), are those which would be measured by each detector if there was no absorption or scattering and the normalised signals, S_n (n=0,1,2,3), are the measured signals in water. The r_n (n=0,1,2,3) are the relative detector response functions as a function of wavelength. a is the absorption coefficient, s is the scattering coefficient, and l is the path length through the probe's water section. Under the assumption that the absorption and scattering of air in the visible wavelength range are negligible when compared to that of the purest waters, the normalised signals, S^n, can be estimated by measuring the normalised signals, S_n^a (n=0,1,2,3), when air is introduced into the probe's water section. The signals are related by

$$S^n = (T_w / T_a)^2 S_n^a \tag{20}$$

where T_w is the transmittance for a quartz to water interface and T_a for a quartz to air interface. To solve (18) and (19) for the absorption and scattering coefficients, a functional form for the cumulative scattering phase function w_f is required. The form given by equation 15 for natural waters will be used in the remainder of this work.

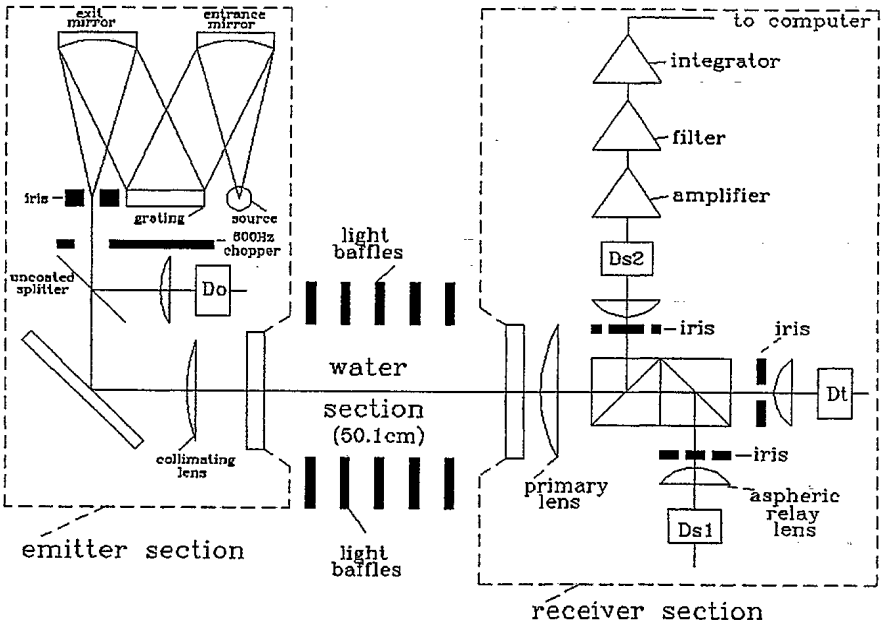

Figure 3. Schematic diagram of the NEARSCAT probe.

The approach outlined above allows one to solve for absorption and scattering at each wavelength separately. To further constrain the fit it is also possible to solve for all wavelengths simultaneously using equation 17 modified to match the notation of equations 19-20.

$$s = s_r \left(\frac{\lambda_r}{\lambda} \right)^{\mu-3} \tag{21}$$

λ_r is an arbitrary reference wavelength and s_r is the value of the total scattering coefficient at this reference wavelength. For the sake of convenience we will in the remainder of this paper use 530 nm as the reference wavelength. Substituting equation 21 back into equations 18-20 we can in theory fit a single set of parameters (s_r, μ, n) to the entire scattering coefficient spectrum. In practise we have found that we need to independently specify the index of refraction n. This is not really too surprising as the only significant effect of this parameter is to fix the large angle portion of the phase function. We use a mean value of 1.09. This value was determined from our fit to the complete data sets of Petzold[5] and Whitlock[6]. The value of the exponent μ is however quite accurately specified by our nephelometer data as this power law exponent is the dominant factor in the narrow forward scattering portion of the phase function, precisely the zone measured by NEARSCAT.

5. DATA ANALYSIS

The spectral data from two West Coast experiments is shown in figure 4 and figure 5. The data were taken in Patricia bay off Vancouver Island on two successive days. The bay is relatively shallow and the NEARSCAT nephelometer was operating 1 meter from the bottom. The absorption spectrum is the same on both days but the scattering coefficient varies by almost a factor of two. We believe this effect is due to the incoming tide scouring the bottom and raising clouds of particles in the first few meters. The index of refraction chosen in our fit to the data was 1.09. The particle size distribution power law (Junge) exponent was 3.579 on January 12 1992 and 3.667 on January 13 1992. Following equations 5 and 6, these exponents give rise to an inverse power dependence of the total scattering coefficient as a function of wavelength of 0.579 and 0.667, respectively.

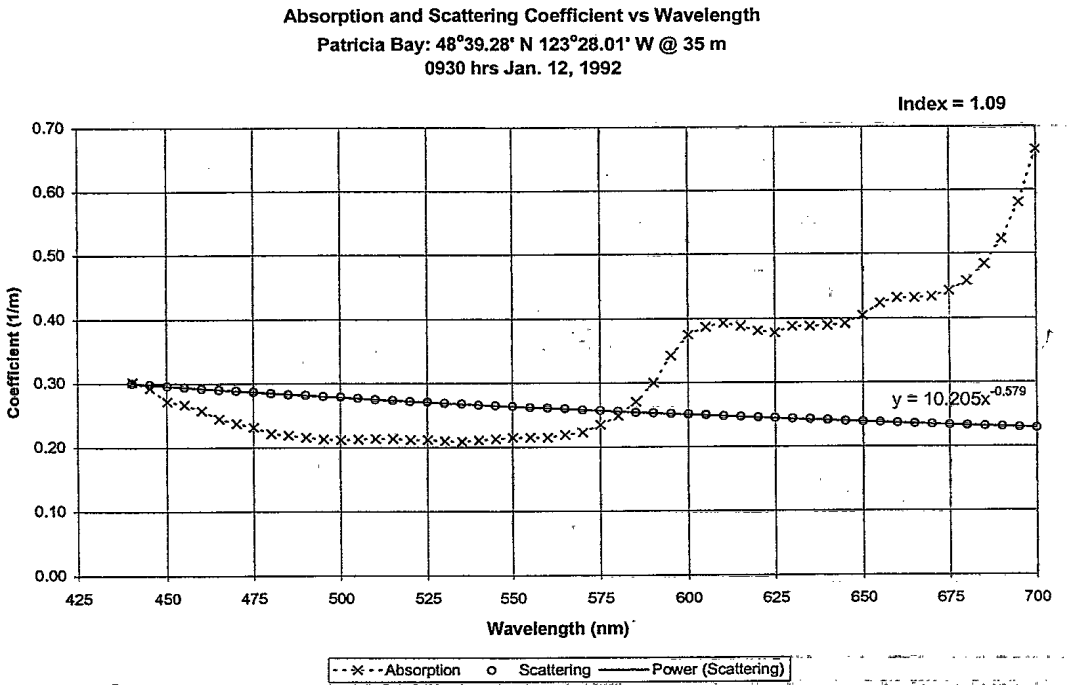

Figure 4. Plot of the spectral dependence of the intrinsic optical coefficients. $\mu = 3.579, n = 1.09$

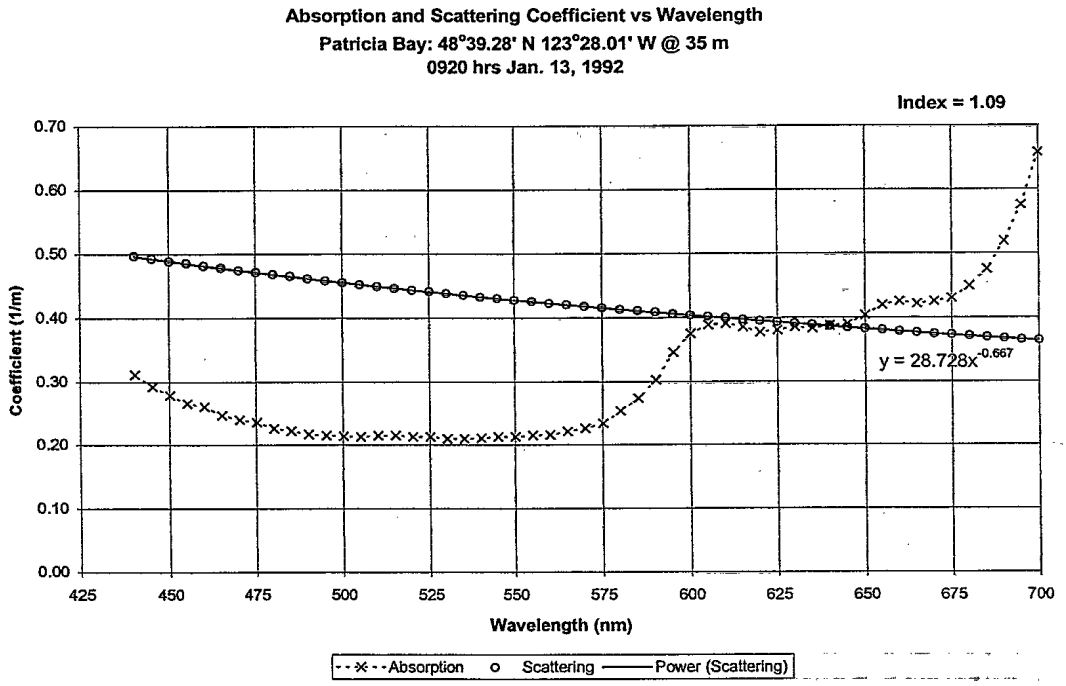

Figure 5. Plot of the spectral dependence of the intrinsic optical coefficients. $\mu = 3.667, n = 1.09$

Figure 6 is a plot of the intrinsic coefficients at 530 nm and of the Junge exponent as a function of depth in an inland channel near Victoria. These results were taken in a mode where six wavelengths are continuously sampled as a function of depth.

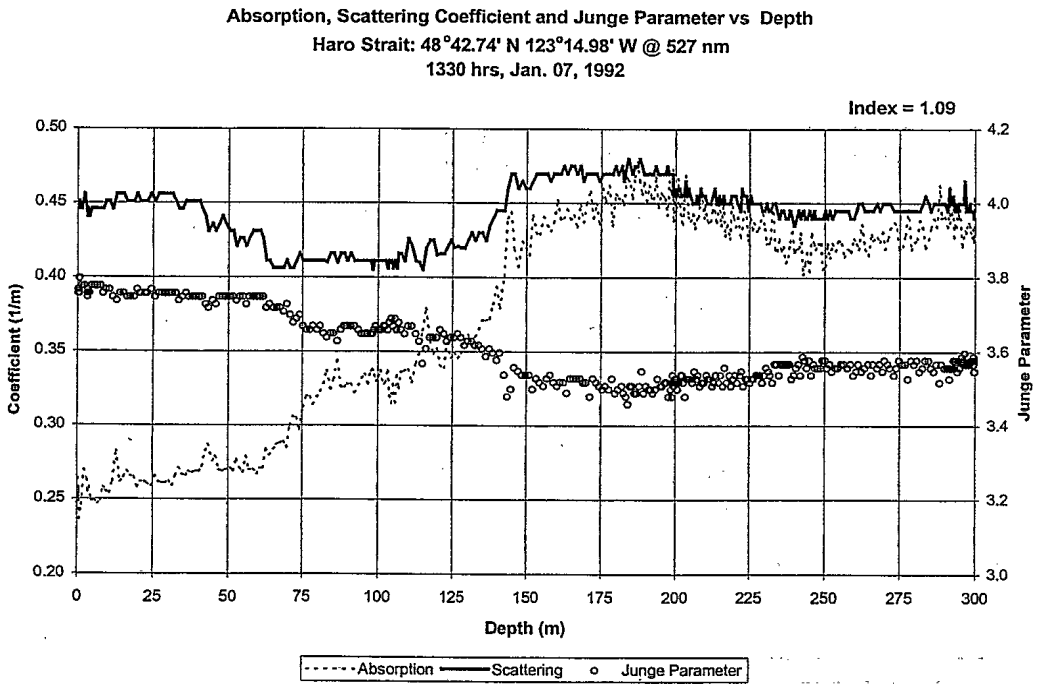

Figure 6. Plot of the intrinsic optical coefficients and Junge exponent as a function of depth.

Note the clear appearance of two zones in the graph. These can be seen as a sharp change in all the parameters at about a depth of 125 meters. The Junge exponent varies from 3.75 near the surface to 3.55 close to the bottom while the absorption goes from 0.26 m^{-1} near the surface to 0.44 m^{-1} at depth.

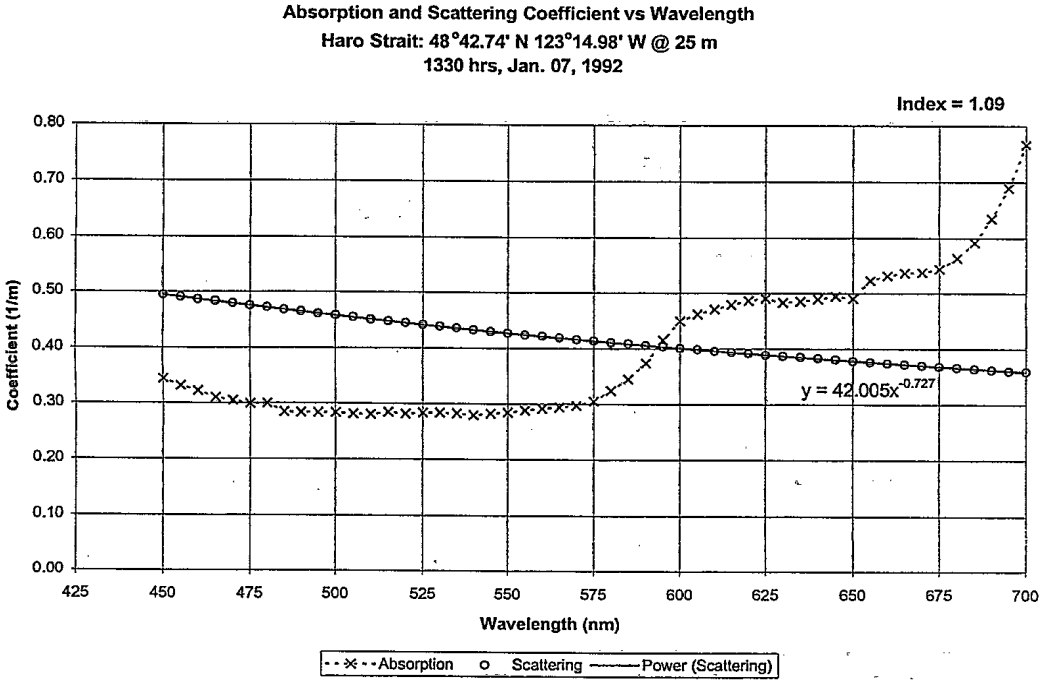

Figure 7. Plot of the spectral dependence of the intrinsic optical coefficients. $\mu = 3.727, n = 1.09$

Figure 7 shows the corresponding spectral dependence measured in the surface layer at a depth of 25 meters. The absorption coefficient is slightly higher than in Patricia bay but its spectral shape has not varied significantly while the scattering coefficient is similar to that obtained on 13 January 1992 in Patricia Bay and shown in figure 5.

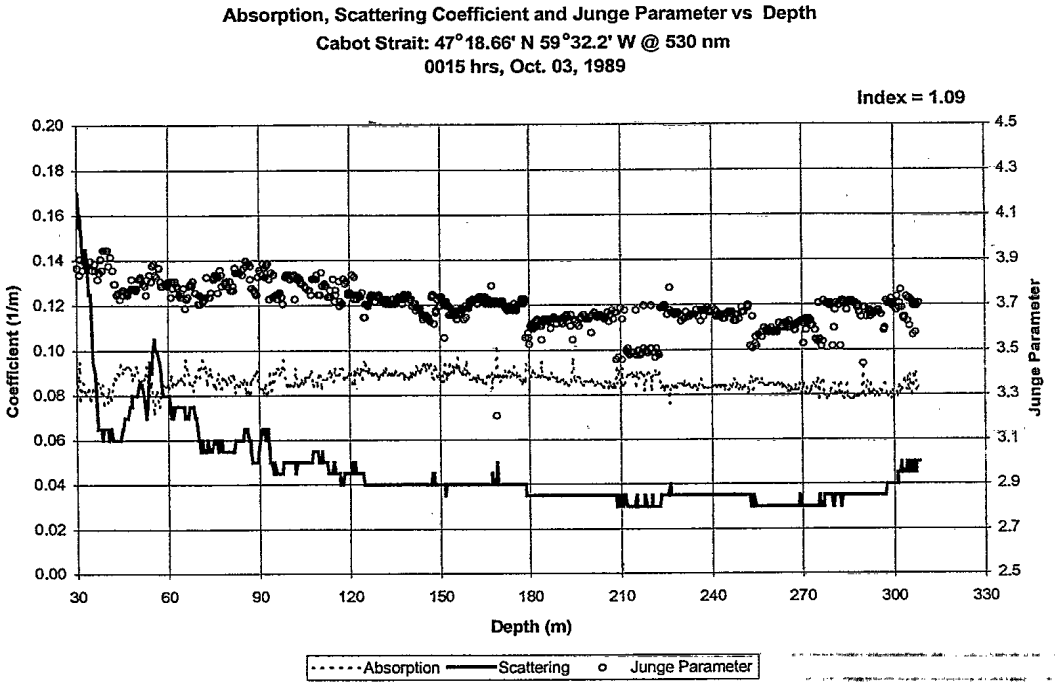

Figure 8. Plot of the intrinsic optical coefficients and Junge exponent as a function of depth

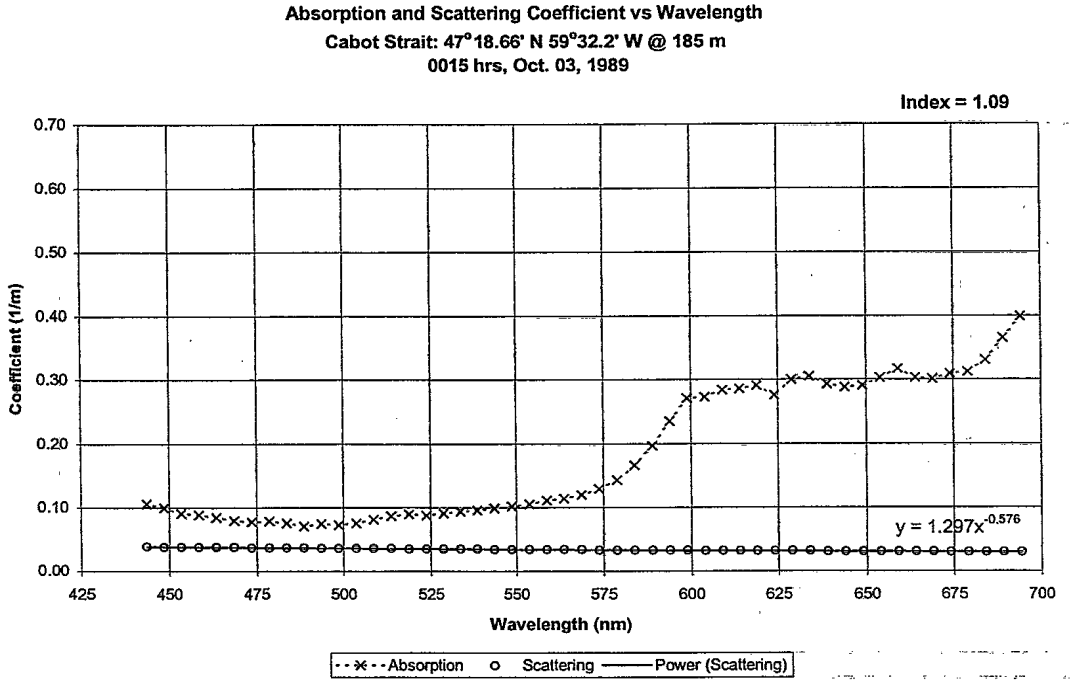

Figure 9. Plot of the spectral dependence of the intrinsic optical coefficients. $\mu = 3.576, n = 1.09$

Figure 8 is a plot of the intrinsic optical coefficients at 530 nm and of the Junge exponent as a function of depth taken in Cabot Strait on the East Coast of Canada. This channel lies between Newfoundland and Nova Scotia where the Gulf of St-Lawrence joins the Atlantic Ocean. In this case from 35 meters up to the surface the scattering is seen to change dramatically. We have seen this increase in scattering near the surface in many of our dives. We generally attribute this to biological activity in the layer above the thermocline. In this particular case our dive was conducted during a storm in an area with 4-meter waves. We believe a large amount of bubbles were entrained in the water column near the surface. We therefore only show in figure 8 the data we believe to be representative of the bulk of the water column. As can be seen, the Junge exponent varies in a substantially linear fashion between 3.9 near the surface and 3.5 at depth. The absorption coefficient is quite uniform at all depths with a value near 0.09 m^{-1} and the scattering coefficient drops significantly from 0.15 m^{-1} near the surface to 0.04 m^{-1} at depth. Figure 9 is a corresponding spectrum taken at a depth of 185 meters and shows the water to be extremely clear with a dominant absorption term. This is in contrast to the inland coastal waters on the West Coast of Canada, where the scattering coefficient at 530 nm was dominant or at best equal to the absorption coefficient in all cases.

6. CONCLUSIONS AND FUTURE WORK

We have developed a phase function formula that can be used to analyze nephelometer data. The formula predicts a simple inverse power form for the spectral dependence of the total scattering coefficient. We successfully verified the accuracy of this form against experimental data. Further analysis of the available data sets of Petzold[5] and Whitlock[6] confirmed that the population distributions gave rise to an average relative index of refraction of 1.09 with a standard deviation of 0.01. For both our East and West Coast data, we found that the mean value of the inverse power law exponent was 3.65 with a standard deviation of 0.12. This implies an inverse power law as a function of wavelength with a mean exponent of $\gamma = 0.65$ with the same standard deviation of 0.12. We are planning to pursue the present work to see what further conclusions can be drawn from our full database of nephelometer results.

7. REFERENCES

1. G.R. Fournier and J.L. Forand, ``Analytic phase function for ocean water'', SPIE Ocean Optics XII , Vol. 2258, pp. 194-201, Bergen, 1994.
2. G.R. Fournier, J.L. Forand, G. Pelletier and P. Pace, ``NEARSCAT full spectrum narrow forward angle transmissometer nephelometer'', SPIE Ocean Optics XI, Vol. 1750, pp. 114-125, San Diego, 1992
3. J.L. Forand ,G.R. Fournier, D. Bonnier, G. Pelletier and P. Pace, ``NEARSCAT: a full spectrum narrow forward angle transmissometer nephelometer'', IEEE Oceans '93, Vol. III, pp. 165-170, Victoria, 1993
4. T.W. Chen, ``Simple formula for light scattering by a large spherical dielectric'', Applied Optics, Vol. 32, pp. 7568 – 7571, 1993
5. T.J. Petzold, ``Volume scattering functions for selected ocean waters'', Scripps Institute of Oceanography, SIO Ref. 72-28 (1972)
6. C.H. Whitlock, L.R. Poole, J.W. Usry, W.M. Houghton, W.D. Morris and E.A. Gurganus, ``Comparison of reflectance with backscatter and absorption parameters for turbid waters'', Applied Optics, Vol. 20, pp. 517-522, 1981
7. J.A. Nelder and R. Mead, Computer Journal, Vol. 7, pp. 308-315, 1965
8. W.H. Press, B.P. Flannery, S.A. Teukolsky and W.H. Vetterling, ``Numerical Recipies in C'', pp. 305-309, Cambridge University Press, 1989
9. A. Morel, ``Optical properties of pure water and pure seawater'', in *Optical Aspects of Oceanography*. N.G. Jerlov and E. Steeman-Nielsen, Academic Press, London, 1974